

Citation for published version:

Bryant, MR, Burrows, AD, Kepert, CJ, Southon, PD, Qazvini, OT, Telfer, SG & Richardson, C 2017, 'Mixed-component sulfone-sulfoxide tagged zinc IRMOFs: In situ ligand oxidation, carbon dioxide, and water sorption studies', *Crystal Growth and Design*. <https://doi.org/10.1021/acs.cgd.7b00007>

DOI:

[10.1021/acs.cgd.7b00007](https://doi.org/10.1021/acs.cgd.7b00007)

Publication date:

2017

Document Version

Peer reviewed version

[Link to publication](https://doi.org/10.1021/acs.cgd.7b00007)

This document is the Accepted Manuscript version of a Published Work that appeared in final form in *Crystal Growth and Design*, copyright © American Chemical Society after peer review and technical editing by the publisher. To access the final edited and published work see: <https://doi.org/10.1021/acs.cgd.7b00007>

University of Bath

Alternative formats

If you require this document in an alternative format, please contact:
openaccess@bath.ac.uk

General rights

Copyright and moral rights for the publications made accessible in the public portal are retained by the authors and/or other copyright owners and it is a condition of accessing publications that users recognise and abide by the legal requirements associated with these rights.

Take down policy

If you believe that this document breaches copyright please contact us providing details, and we will remove access to the work immediately and investigate your claim.

Mixed-component sulfone–sulfoxide tagged zinc IRMOFs: *In situ* ligand oxidation, carbon dioxide and water sorption studies

Macguire R. Bryant[†], Andrew D. Burrows[‡], Cameron J. Kepert[§], Peter D. Southon[§], Shane G. Telfer^{||}, and Christopher Richardson^{†}*

[†]School of Chemistry, University of Wollongong, Northfields Avenue, Wollongong NSW 2522, Australia

[‡]Department of Chemistry, University of Bath, Claverton Down, Bath BA2 7AY, United Kingdom

[§] School of Chemistry, University of Sydney, Sydney NSW 2006, Australia

^{||} MacDiarmid Institute for Advanced Materials and Nanotechnology, Institute of Fundamental Sciences, Massey University, Palmerston North, New Zealand

ABSTRACT

Reported here are the syntheses and sorption properties of a series of single- and mixed-component zinc IRMOFs derived from controlled ratios of sulfide and sulfone functionalized linear biphenyldicarboxylate (bpdc) ligands. During MOF synthesis the sulfide moieties undergo

in situ oxidation, giving rise to sulfoxide functionalized ligands which are incorporated to give mixed-component sulfoxide-sulfone functionalized MOFs. The single- and mixed-component systems all share the IRMOF-9 structure type as determined by a combination of single crystal and powder X-ray diffraction analyses. The functionalized IRMOF-9 series was investigated by N₂ and CO₂ gas adsorption and by water vapor sorption measurements. MOFs containing higher proportions of sulfoxide have slightly larger accessible surface areas and pore volumes whereas MOFs containing a greater proportion of the sulfone functionality demonstrated higher CO₂ adsorption capacities, enthalpies of CO₂ adsorption and CO₂/N₂ selectivities. Water sorption studies at 298 K showed the MOFs to have pore-filling steps starting around 0.4 P/P_0 . In general, only small changes in water adsorption were observed with regards to ligand ratios in the mixed-component MOFs, suggesting primary effects are dominated by pore size. A ligand-directed fine-tuning approach of changing alkyl chain length was demonstrated to give smaller more hydrophobic pores with better adsorption characteristics.

INTRODUCTION

Metal-organic frameworks (MOFs) are porous crystalline materials with promise in applications such as heterogeneous catalysis,¹ chemical sensing² and molecular separations.³ Research into MOFs is developing rapidly because the size and shape⁴ and chirality⁵ of their pores. Additionally, the chemical properties of the pore surfaces can be rationally engineered via modular synthetic methods.⁶ This grants a great deal of control over the pore characteristics of the MOF through judicious choice of organic ligands and metal centers.^{4b, 6c, 7}

The sorption of gases by MOFs has seen a large amount of interest,⁸ particularly the selective adsorption of CO₂ for carbon capture and remediation applications.^{8a, 9} One strategy is to use functional groups attached to the bridging ligands as sites for strong and selective binding of

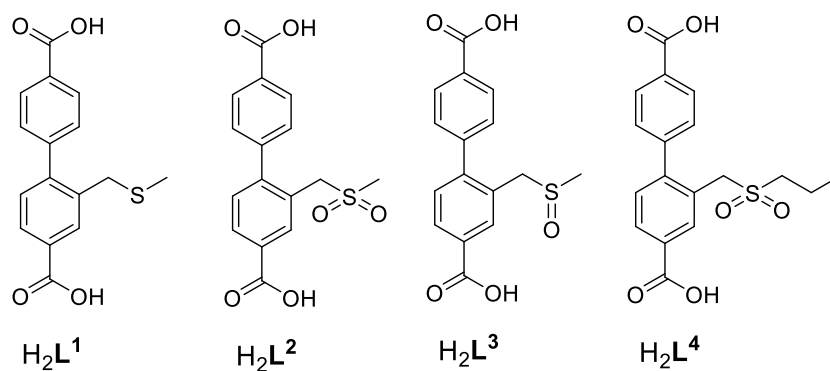
CO₂,¹⁰ and a clear trend is an increase in CO₂ binding strength with increasing polarizability of the groups.¹¹ However, these types of functional groups also tend to interact strongly with water. In situations where CO₂ and water might be found together, such as in flue streams, this would lead to competitive adsorption.¹² There are also documented problems of many MOFs degrading upon contact with water.¹³ This means a critical marker for the application of MOFs is the relative humidity at which pore-filling occurs. Removal of the pore-water can stress frameworks to collapse.¹⁴ In order to make MOFs useful materials, fashioning pore surfaces to repel water while maintaining favorable properties for adsorbing CO₂ is important.^{8a, 15} Strategies to repel water include functionalization of MOF pore space with fluorine-containing groups¹⁶ and alkyl chains.¹⁷

One approach to chemically fine tune MOFs is by forming mixed-component MOFs (MC-MOFs; also known as multivariate or MTV-MOFs), where structurally similar yet differently functionalized ligands are incorporated to the lattice.¹⁸ We have shown that the compositions of MC-IRMOF-1-type frameworks can be controlled by the reaction time.^{18c} Moreover, this approach offers the potential to tune the properties of the materials. For example, sorption of H₂, CO₂ and CO are enhanced by combining allyloxy- and benzyloxy- functionalities in MC-IRMOF-1-type frameworks.^{18d} Differences in CO₂ and water adsorption were shown to depend on bdc/bdc-NH₂/bdc-NO₂ linker proportions in MC-MIL-101(Cr) MOFs.¹⁹ In bpy-pillared zinc isophthalate MC-MOFs, the ratios of methoxy- and nitro-functionalized ligands could be tuned to improve the adsorption of CH₄ over CO₂ and C₂H₆.²⁰ Interestingly, while MC-MOFs can engender differences in properties, the responses are not always products of linear combinations of the linker components. For example, the best H₂ adsorption performance of bdc/bdc-OMe MC-IRMOF-1 was with 25% bdc-OMe incorporation²¹ and the highest surface area of bdc/bdc-

NH₂ MC-IRMOF-1/3 frameworks was achieved with 25% bdc-NH₂.²² The complex nature yet clear potential to create superior materials through a MC approach is an aspect of MOF chemistry which requires additional research.

In previous work we found that zinc MOFs made from thioether-tagged ligand H₂L¹ and sulfone-tagged ligand H₂L² (Chart 1) share the interpenetrated IRMOF-9 structure type.²³ More recently we investigated the sulfoxide-tagged ligand L³ in an IRMOF-9 type framework for its thermally-induced post-synthetic elimination chemistry.²⁴ Here we desired to create a series of MC-IRMOF-9 compounds with controlled proportions of relatively non-polar sulfide and polar sulfone groups and probe CO₂ adsorption and the influence the chemical functionality has on water adsorption properties. We considered that flexible tethers containing polar functional groups together with short alkyl chains could strike the right balance between good interactions with CO₂ and pore hydrophobicity. MOFs containing sulfide ligands have been shown to be relatively hydrophobic,²⁵ while sulfone-containing MOFs have good CO₂ binding properties.^{11c, 26} Similarly, the sulfone group is also well used in CO₂ adsorbing polymers and membrane materials.²⁷

Chart 1. Structures of ligands H₂L¹⁻⁴.



EXPERIMENTAL METHODS

MOFs MSO₂Me-15 (WUF-6; WUF, Wollongong University Framework) and MSO₂Me-100 were prepared as reported in the literature.²³⁻²⁴ All chemicals used were of analytical grade and purchased from either Sigma Aldrich, VWR Australia or Ajax Finechem Pty Ltd. ¹H NMR and ¹³C NMR spectra were obtained using a Varian Mercury VX-300-MHz NMR spectrometer operating at 300 MHz for ¹H and 75.5 MHz for ¹³C, or a Varian Inova-500-MHz NMR spectrometer, operating at 500 MHz for ¹H and 125 MHz for ¹³C. ¹H NMR spectra were referenced to the residual *protio* peaks at δ 2.50 ppm (*d*₆-DMSO) or δ 7.27 ppm in CDCl₃. ¹³C NMR spectra were referenced to the solvent peaks at δ 39.6 ppm in *d*₆-DMSO or δ 77.7 ppm in CDCl₃. For ¹H NMR analysis, MOF samples (~10 mg) were digested by adding 35% DCl in D₂O (2 μ L) and *d*₆-DMSO (500 μ L) and stirring until a solution was obtained.

Simultaneous thermogravimetric and differential thermal analysis (TG-DTA) data were obtained using a Shimadzu DTG-60 instrument fitted with a FC-60A flow rate controller and TA-60WS thermal analyzer. Measuring parameters of 10 °C per min under nitrogen flow (20 cm³ min⁻¹) were used. Powder X-ray diffraction (PXRD) patterns were recorded on a GBC-MMA X-ray diffractometer with samples mounted on 1" SiO₂ substrates. Experimental settings in the 2 θ angle range of 3–30° of 0.04° step size and a scan speed of 3° min⁻¹ were used.

Single crystal X-ray diffraction (SCXRD) data were recorded on a Rigaku Spider diffractometer equipped with a MicroMax MM007 rotating anode generator (Cu radiation, 1.54180 Å), fitted with high flux Osmic multilayer mirror optics, and a curved image-plate detector. Data were collected at 293 K and were integrated and scaled and averaged with FS process.²⁸ XPREP was used to determine the space group and the structure was solved using SHELXS and refined with SHELXL.²⁹ Details on the refinement can be found in the SI to this

article. Data are deposited with the Cambridge Structural Database (CCDC 1503491). Data can be obtained for free from www.ccdc.cam.ac.uk

Gas sorption studies up to 1 bar were carried out using a Quantachrome Autosorb MP instrument and high purity nitrogen (99.999 %) and carbon dioxide (99.995 %) gases at the Wollongong Isotope and Geochemistry Laboratory. Surface areas were determined using Brunauer-Emmett-Teller (BET) calculations. Vapor and gas sorption studies up to 10 bar were carried out on a Hiden Isochema IGA-002 Single Component Gas and Vapor Sorption Analyzer. Elemental microanalysis was performed by the Microanalytical Unit at the Australian National University using a Carlo Erba 1106 automatic analyzer, and the Elemental Microanalysis Service at Macquarie University using a PerkinElmer Elemental Analyzer, Model PE2400 CHNS/O. Each sample was heated at 110 °C for 2 h and analyzed immediately afterward.

Synthetic procedure for H₂L⁴

Synthesis of dimethyl 2-((propylthio)methyl)-[1,1'-biphenyl]-4,4'-dicarboxylate

Propanethiol (200 μ L, 2.2 mmol) and then Et₃N (150 μ L, 1.1 mmol) were added to dimethyl 2-(bromomethyl)-[1,1'-biphenyl]-4,4'-dicarboxylate (278 mg, 0.76 mmol) in CH₂Cl₂ (3 cm³) with stirring. After 5 days the reaction was worked up by dilution with CH₂Cl₂ (5 cm³) washing with aqueous NaOH (0.25 M), brine, drying over Na₂SO₄ and rotary evaporation. The residue was assayed by NMR spectroscopy and showed only product (*R_f* 0.82, 1–1 CH₂Cl₂–Hexane). ¹H NMR δ_{H} /ppm (500 MHz; CDCl₃) 0.90 (3 H, t, *J* = 7.25 Hz), 1.47 (2 H, q, *J* = 7.25 Hz), 2.38 (2 H, t, *J* = 7.25 Hz), 3.67 (2 H, s), 3.96 (6 H, s), 7.31 (1 H, d, *J* = 8.00 Hz), 7.51 (2 H, d, *J* = 8.00 Hz), 7.96 (1 H, d, *J* = 8.00 Hz), 8.13 (3 H, m). ¹³C NMR δ_{C} /ppm (125 MHz; CDCl₃) 14.04, 23.26, 34.46, 35.18, 52.89, 127.92, 128.77, 129.86, 130.18, 130.22, 130.54, 130.86, 132.20, 137.07, 145.51, 146.12, 167.34, 167.50.

Synthesis of dimethyl 2-((propylsulfonyl)methyl)-[1,1'-biphenyl]-4,4'-dicarboxylate

The residue obtained above was taken up in AcOH (3 cm³) and 30% H₂O₂ (0.5 cm³, 4.4 mmol) was added drop wise with stirring. The mixture was heated to 80 °C for one hour and after cooling most of the AcOH was removed by rotary evaporation. The product was precipitated by the addition of water, separated by filtration, washed with water, air dried, and crystallized from MeOH/H₂O (*R_f* 0.35, 1–1 CH₂Cl₂–Hexane). ¹H NMR δ_H/ppm (500 MHz; CDCl₃) 0.95 (3 H, t, *J* = 7.50 Hz), 1.62 (2 H, m), 2.70 (2 H, t, *J* = 8.00 Hz), 3.96 (6 H, s), 4.28 (2 H, s), 7.41 (1 H, d, *J* = 8.00 Hz), 7.47 (2 H, d, *J* = 8.00 Hz), 8.11 (1 H, d, *J* = 5.00 Hz), 8.15 (2 H, d, *J* = 5.00 Hz), 8.32 (1 H, s). ¹³C NMR δ_C/ppm (125 MHz; CDCl₃) 13.69, 16.34, 53.00, 53.08, 55.17, 56.02, 126.25, 130.07, 130.60, 130.70, 130.73, 131.04, 131.42, 133.64, 144.59, 147.59, 166.82, 167.23.

Synthesis of 2-((propylsulfonyl)methyl)-[1,1'-biphenyl]-4,4'-dicarboxylic acid (H₂L⁴)

1M NaOH solution (0.690 cm³, 0.690 mmol) was added dropwise to dimethyl 2-((propylsulfonyl)methyl)-[1,1'-biphenyl]-4,4'-dicarboxylate (107.65 mg, 0.276 mmol) dissolved in MeOH (5.5 cm³) and THF (1 cm³) and left to stir for 18 hours. The solution was filtered and the MeOH and THF were removed by rotary evaporation before dilution with water (10 cm³) and acidification with 1M HCl. The precipitated solid was separated by filtration, washed with water (3 × 10 cm³), and air dried overnight. Yield = 87.3 mg (86 %). ¹H NMR δ_H/ppm (500 MHz; *d*₆-DMSO) 0.84 (3 H, t, *J* = 7.50 Hz), 1.56 (2 H, m), 2.90 (2 H, t, *J* = 7.50 Hz), 4.45 (2 H, s), 7.46 (1 H, d, *J* = 8.00 Hz), 7.54 (2 H, d, *J* = 7.50 Hz), 8.02 (3 H, m), 8.15 (1 H, s), 13.12 (2 H s). ¹³C NMR δ_C/ppm (125 MHz; *d*₆-DMSO) 12.71, 15.40, 54.11, 126.07, 129.34, 129.48, 129.53, 129.77, 130.18, 130.22, 130.51, 130.97, 133.60 (br), 143.60, 146.56, 166.79, 167.11.

General synthetic procedure for MSO₂Me-36, MSO₂Me-64, MSO₂Me-79

The requisite amounts of Zn(NO₃)₂·6H₂O, H₂L¹ and H₂L² were stirred in *N,N'*-dimethylformamide (DMF) (16 cm³) until a solution was obtained. The solution was placed in an oven pre-heated to 100 °C for 24 hours. The DMF solution was then exchanged three times for fresh DMF (2 cm³) at 100 °C, then at room temperature for CH₂Cl₂ over 3 days, and then for benzene over 2 days. The samples were activated by freeze drying at –53 °C and 0.09 mbar for 1 hour followed by heating under dynamic vacuum at 120 °C for 5 hours.

Data for MSO₂Me-36 (WUF-7)

Zn(NO₃)₂·6H₂O (267.0 mg, 0.897 mmol), H₂L¹ (67.8 mg, 0.224 mmol), H₂L² (25.0 mg, 0.075 mmol); Yield 49 %; Elemental analysis of MSO₂Me-36 [Zn₄O(L²)_{1.08} (L³)_{1.92}(H₂O)_{0.75}]: calc. C: 45.86%, H: 3.01%, S: 7.63%, N: 0.00%; Found C: 46.10%, H: 3.28%, S: 6.76%, N: 0.00%.

Data for MSO₂Me-64 (WUF-8)

Zn(NO₃)₂·6H₂O (294 mg, 0.987 mmol), H₂L¹ (49.8 mg, 0.165 mmol), H₂L² (55.2 mg (0.165 mmol); Yield 56 %; Elemental analysis of MSO₂Me-65 [Zn₄O(L²)_{1.92} (L³)_{1.08} (H₂O)₂]: calc. C: 44.59%, H: 3.12%, S: 7.42%, N: 0.00%, Found C: 44.12%, H: 3.09%, S: 7.26%, N: 0.00%

Data for MSO₂Me-79 (WUF-9)

Zn(NO₃)₂·6H₂O (266.8 mg, 0.897 mmol), H₂L¹ (22.6 mg, 0.075 mmol), H₂L² (75.0 mg, 0.224 mmol); Yield 60 %; Elemental analysis of MSO₂Me-79 [Zn₄O(L²)_{2.38}(L³)_{0.62}(H₂O)₂]: calc. C: 44.34%, H: 3.10%, S: 7.38%, N: 0.00%, Found C: 44.12%, H: 3.09%, S: 7.26%, N: 0.00%.

Synthetic procedure for MSO₂Pr-100 (WUF-10)

Zn(NO₃)₂·6H₂O (70.5 mg, 0.237 mmol) and H₂L⁴ (28.7 mg, 0.079 mmol) were stirred in DMF (4 cm³) until a solution was obtained. The solution was placed in an oven pre-heated to 100 °C for 24 hours. The crystals were treated in the same manner as in the general procedure. Elemental

analysis of MSO₂Pr-100 [Zn₄O(L⁴)₃(H₂O)]: calc. C: 47.12%, H: 3.66%, S: 6.97%, N: 0.00%, Found C: 47.07%, H: 3.41%, S: 6.71%, N: 0.00%.

RESULTS

Synthesis and Characterization

A series of five functionalized MC-IRMOF-9 analogues containing **L**² and **L**³ (denoted MSO₂Me-X, where X represents the percentage of sulfone ligand **L**² in the structure) were prepared by direct solvothermal syntheses reacting Zn(NO₃)₂·6H₂O with defined ratios of H₂**L**¹ and H₂**L**² (Table 1) over 24 hours in DMF at 100 °C. Single-component MSO₂Pr-100 was prepared similarly by direct solvothermal synthesis from Zn(NO₃)₂·6H₂O and H₂**L**⁴. In order to determine the proportions of each ligand in the MC-MOFs, samples were solvent exchanged and activated before digestion in DCl and *d*₆-DMSO for analysis using ¹H NMR spectroscopy. The spectra show no **L**¹ is present in the MC-MOFs (Figure 1) as the characteristic methyl (δ 1.91 ppm) and methylene signals (δ 3.71 ppm) for this compound are absent. Instead, the presence of the sulfoxide-tagged ligand **L**³ (Chart 1) is confirmed by the appearance of doublets at δ 4.04 and δ 4.14 ppm for the methylene protons. This indicates that during MC-MOF synthesis, H₂**L**¹ is converted completely by oxidation. The ¹H NMR data was used to calculate the relative incorporation of the ligands in the MC MOFs, allowing the compositions of the frameworks to be formulated (Table 1).

We have previously reported MSO₂Me-15 (WUF-6), which although being prepared solely from sulfoxide ligand H₂**L**³ contains 15% of the sulfone **L**² in its structure. We ascribed this to occur via disproportionation–re-oxidation pathways during MOF synthesis.²⁴ Considering this result, the increased incorporation of **L**² into MSO₂Me-36 (-64) and (-79) relative to the starting

synthetic ratio arises from the *in situ* oxidation chemistry, rather than via a selective incorporation of \mathbf{L}^2 over $\mathbf{L}^1/\mathbf{L}^3$.

Table 1. Starting synthetic ratios, percentage compositions and framework formulations of the MOFs synthesized in this work.

MOF	$H_2\mathbf{L}^1 : H_2\mathbf{L}^2$ synthesis ratio (mol%)	Ligand incorporation in MOF (mol%) ^a		Framework Formulation
		\mathbf{L}^2	\mathbf{L}^3	
MSO ₂ Me-15	- ^b	15	85	$Zn_4O(\mathbf{L}^2)_{0.45}(\mathbf{L}^3)_{2.55}$
MSO ₂ Me-36	75 : 25	36	64	$Zn_4O(\mathbf{L}^2)_{1.08}(\mathbf{L}^3)_{1.92}$
MSO ₂ Me-64	50 : 50	64	36	$Zn_4O(\mathbf{L}^2)_{1.92}(\mathbf{L}^3)_{1.08}$
MSO ₂ Me-79	25 : 75	79	21	$Zn_4O(\mathbf{L}^2)_{2.38}(\mathbf{L}^3)_{0.62}$
MSO ₂ Me-100	0 : 100	100	0	$Zn_4O(\mathbf{L}^2)_3$
MSO ₂ Pr-100	- ^c	-	-	$Zn_4O(\mathbf{L}^4)_3$

^a As determined through ¹H NMR spectroscopy. ^bMSO₂Me-15 was synthesized starting from $H_2\mathbf{L}^3$ only. ^cMSO₂Pr-100 was synthesized starting from $H_2\mathbf{L}^4$ only.

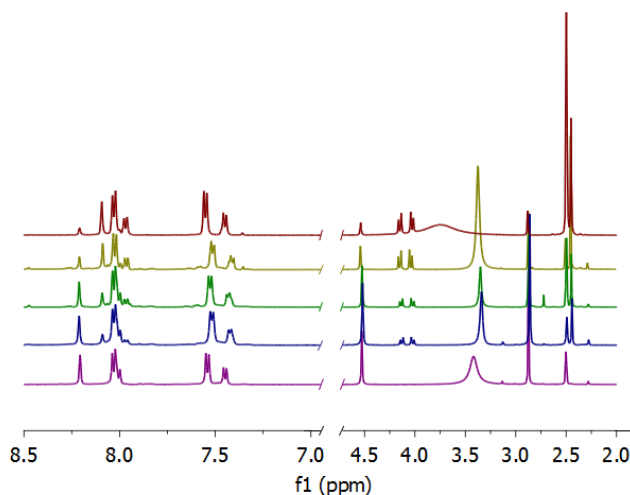


Figure 1. ^1H NMR spectra of digested samples of $\text{MSO}_2\text{Me-15}$ (red), $\text{MSO}_2\text{Me-36}$ (yellow), $\text{MSO}_2\text{Me-64}$ (green), $\text{MSO}_2\text{Me-79}$ (blue), and $\text{MSO}_2\text{Me-100}$ (purple).

The crystallinity of the activated MOFs was analyzed by PXRD and the patterns are shown in Figure 2. Previously, $\text{MSO}_2\text{Me-100}$ was shown by SCXRD to have the doubly interpenetrated framework structure of IRMOF-9.²³ The MC-MOFs in this series all show peaks in identical two-theta positions and with similar intensities to activated $\text{MSO}_2\text{Me-100}$, signifying that all are isostructural with the interpenetrated IRMOF-9 structure type. After exposure to the atmosphere these patterns change quickly and eventually show no peaks, indicating poor stability of these MOFs against atmospheric moisture. This has been observed previously for MOFs with Zn_4O nodes^{13c} and for similarly functionalized frameworks.²⁴

Additionally, $\text{MSO}_2\text{Pr-100}$ was analyzed by SCXRD. The framework crystallizes in the space group $C2/m$, as a pair of interpenetrated *pcu* frameworks. We and others have seen IRMOF-9-type structures crystallize in this space group with a variety of tagged biphenyl dicarboxylate (bpdc) ligands.³⁰ The sulfone tag groups were not located in the refinement and this is likely due to being positionally and conformationally disordered within the crystal structure. The PXRD

pattern of MSO₂Pr-100 matches that calculated from the SCXRD structure and the other members of the series (Figure 2).

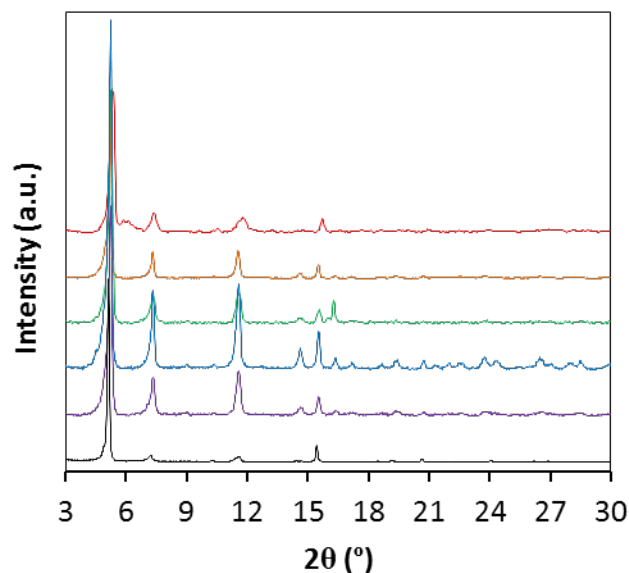


Figure 2. PXRD patterns of MSO₂Me-15 (a), MSO₂Me-36 (b), MSO₂Me-64 (c), MSO₂Me-79 (d), MSO₂Me-100 (e) and MSO₂Pr-100 (f).

The activated MOFs were analyzed by TG-DTA (Figure 3; SI Figures S9-S14). These show that 1-5 % of mass is lost below 100 °C. We attribute this to water adsorbed during transfer and handling of the activated MOFs in air for a short time. Masses are maintained until approximately 235 °C, at which point the small mass losses observed are coupled with exotherms, the magnitude of which is related to the content of sulfoxide **L**³ linkers in the MC-MOFs. For MSO₂Me-15 we established the exotherm and mass loss corresponds to an elimination reaction of methanethiol from **L**³ to generate aldehyde groups and this process occurs for all the MC-MOFs here.²⁴ No exotherm or mass loss is observed for MSO₂Me-100 and

MSO₂Pr-100 as these MOFs contain no **L**³. We have employed TG-DTA to detect post-synthetic reactions inside other MOFs.^{30b, 31}

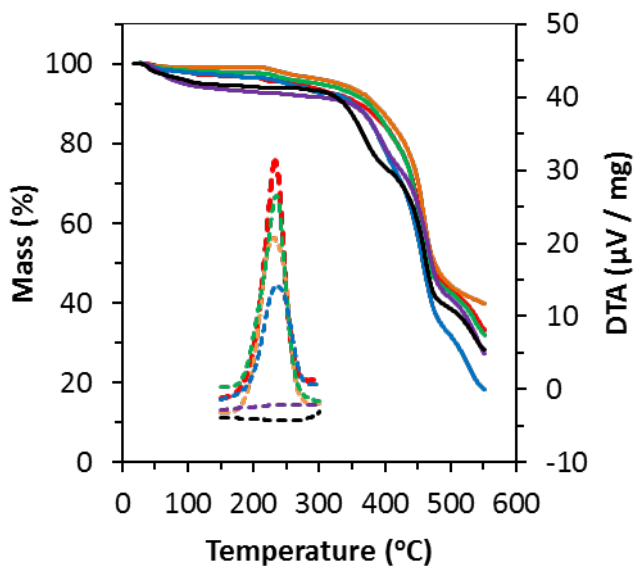


Figure 3. Full TG traces (solid lines) with partial inset DTA traces (dotted lines) for MSO₂Me-15 (red), MSO₂Me-36 (orange), MSO₂Me-64 (green), MSO₂Me-79 (blue), MSO₂Me-100 (purple) and MSO₂Pr-100 (black).

N₂ Gas Sorption

In order to further characterize the MOFs, N₂ gas sorption experiments at 77 K were carried out. All the MOFs show Type I isotherms (Figure 4a; SI Figures S15-S20) with relatively small variations in maximum adsorption, surface areas and pore volumes (Table 2). MSO₂Me-15 possesses the largest surface area, followed by MSO₂Me-64, with MSO₂Me-36 (-79) and (-100) having very similar surface areas. MSO₂Pr-100 displays a smaller surface area than the other MOFs, due to the longer alkyl chain of the incorporated **L**⁴ ligands. Pore size distributions from DFT analysis of the isotherm data indicate that MSO₂Me-15, (-36) and (-64) share pore sizes around 10 Å in diameter, while MSO₂Me-79, MSO₂Me-100 and MSO₂Pr-100 have slightly

smaller, more narrowly distributed pores around 9.6 Å in diameter (Figure 4b). The accessible surface areas and pore size distributions are correlated with the slightly lower pore volumes of MSO₂Me-79 and MSO₂Me-100 and the lower values for MSO₂Pr-100.

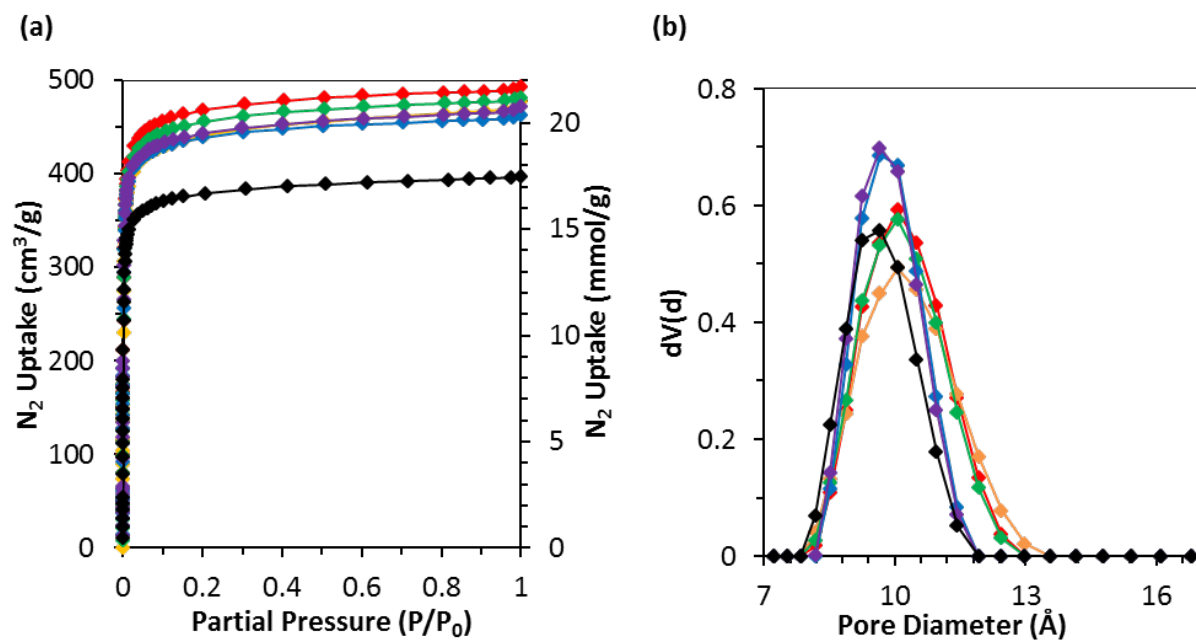


Figure 4. (a) N₂ adsorption isotherms at 77 K and (b) pore size distributions for MSO₂-15 (red), MSO₂Me-36 (orange), MSO₂Me-64 (green), MSO₂Me-79 (blue), MSO₂Me-100 (purple) and MSO₂Pr-100 (black).

Table 2. Characteristics of the MOFs derived from gas sorption experiments

MOF	Apparent Surface Area (m ² /g) ^a	N ₂ Pore Volume (cm ³ /g) ^b	CO ₂ /N ₂ Selectivity at 298 K ^c	CO ₂ Pore Volume (cm ³ /g) ^d
MSO ₂ Me-15	1888	0.76	9.2	0.82
MSO ₂ Me-36	1762	0.74	9.3	0.82
MSO ₂ Me-64	1827	0.74	7.6	0.79
MSO ₂ Me-79	1763	0.72	8.4	0.78

MSO ₂ Me-100	1776	0.73	9.8	0.78
MSO ₂ Pr-100	1514	0.62	15.8	0.65 ^c

^a BET analysis from N₂ adsorption at 77 K (see SI). ^b At P/P₀ 0.995 and 77 K. ^c Derived from the equation $(q_{CO_2})/(q_{N_2}) / (p_{CO_2})/(p_{N_2})$ where $p_{N_2} = 0.75$ and $p_{CO_2} = 0.15$ bar, and q = quantity of adsorbed gas at pressure p and 298 K. ^d At 0.7 bar and 196 K. ^e At 0.6 Bar and 196 K.

CO₂ Gas Sorption

The CO₂ isotherms of each MOF were recorded at 196 K (SI Figure S21) and show equivalent uptake capacities to the N₂ isotherms at 77 K and only small differences in performance between the MOFs. MSO₂Me-15 and (-36) show increased CO₂ uptake than the other frameworks and this is most likely due to their slightly greater pore volumes (Table 2). However, MSO₂Me-100 and (-79) demonstrate increased CO₂ pore filling at lower pressures when compared with MSO₂Me-15, (-36) and (-64). MSO₂Pr-100 demonstrates similar CO₂ adsorption behavior albeit with a smaller maximum amount of adsorbed CO₂, in line with its lower accessible surface area.

The CO₂ adsorption properties of the MOFs were recorded at 273 K, 288 K and 298 K up to 1 bar (SI Figures S22-S27). The adsorption data at 298 K for all MOFs is shown in Figure 5a as a representative example. All samples show essentially linear adsorption, with MSO₂Me-100 having the highest CO₂ adsorption capacity of all the samples and MSO₂Me-15, (-36), (-64) and MSO₂Pr-100 all possessing similar CO₂ uptake capacities. This trend is consistent at each measurement temperature. MSO₂Me-100 and MSO₂Me-79 possess the highest capacities for CO₂. This is notable given these MOFs achieve greater CO₂ adsorption than other MC-MOFs with larger available pore space and surface area. Another conspicuous result is that MSO₂Pr-100 achieves gravimetric CO₂ uptake comparable to MSO₂Me-15 and (-64) despite a lower accessible surface area. Overall, the materials with the highest proportions of sulfone functionality possess the highest CO₂ capacities.

The enthalpy of CO₂ adsorption was calculated from data recorded at 273, 288 and 298 K (Figure 5b). MSO₂Me-79 has an enthalpy of adsorption around 25 kJ mol⁻¹ out to CO₂ loadings of 1 mmol g⁻¹. MSO₂Me-15, (-64), (-100) and MSO₂Pr-100 share similar enthalpies across all loadings (17-19 kJ mol⁻¹) and MSO₂-36 displays a lower enthalpy across higher loadings of CO₂ (~15 kJ mol⁻¹). These values are similar to dimethoxy, dihydroxyl and diiodo functionalized IRMOF-9 compounds.[ref 34]

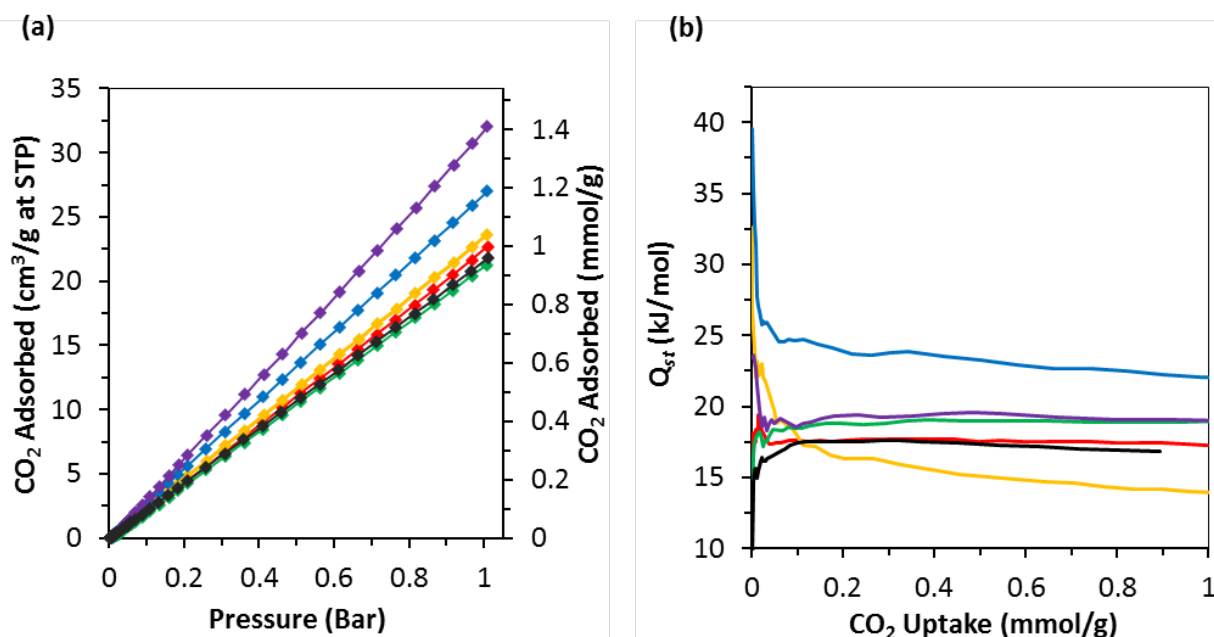


Figure 5. (a) CO₂ adsorption isotherms at 298 K and (b) enthalpy of CO₂ adsorption for MSO₂Me-15 (red), MSO₂Me-36 (orange), MSO₂Me-64 (green), MSO₂Me-79 (blue), MSO₂Me-100 (purple) and MSO₂Pr-100 (black).

CO₂/N₂ selectivity factors were calculated based on single-component CO₂ (Figure 5a) and N₂ (Figure S28) isotherms at 298 K and a theoretical gas mixture of 15% CO₂, 75% N₂, and 10% other gases (Table 2). The MOF with the highest selectivity factor was MSO₂Pr-100 (15.8), followed by MSO₂Me-100 (9.8), MSO₂Me-36 (9.3), MSO₂Me-15 (9.2), MSO₂-79 (8.4) and finally MSO₂-64 (7.6). The higher selectivity of MSO₂Pr-100 can be attributed to a combination

of good CO₂ adsorption performance and a reduction in N₂ adsorption (Figures S27-S28). The good performance of MSO₂Pr suggests the smaller pore size and more hydrophobic pore environment by incorporating the propyl group is favorable for selective CO₂ adsorption.

With regards to the MC-MOFs, there is no clear trend between the sulfoxide-sulfone ratio and selectivity factor. The CO₂/N₂ selectivities are comparable to other MOF materials. For example, the bpdc linked UiO-67 possesses two sizes of pores (11 Å and 8 Å diameter) and a selectivity of 9.4. However, incorporating a sulfone group into the bpdc linker is reported to increase the selectivity to 31.5.^{6d}

To observe performance at higher pressures, CO₂ isotherms were acquired at 298 K up to 10 bar (Figure S29) in which the MOFs all perform similarly with maximum uptakes between 170–200 cm³/g. However, MSO₂Me-79 now outperforms MSO₂Me-100 in uptake capacity, and the isotherm of the latter shows some curvature indicating it is approaching saturation. Also notable is the good performance of MSO₂Pr-100 which shows an uptake capacity comparable to the higher surface area MOF, MSO₂Me-15.

Water Vapor Adsorption

The MOFs were analyzed for their water vapor sorption properties at 298 K (Figure 6, Table 3). We were particularly interested in the performance for water adsorption given the mixture of polar functional groups. In previous work, sulfoxide-containing MOFs were shown to be more hydrophilic than their sulfone counterparts.²⁵ MSO₂Me-15 shows the highest uptake of water vapor below 0.3 P/P_0 , indicating water is more easily adsorbed onto the surface compared with the other MOFs. On the other hand, MSO₂Pr-100 shows the least uptake in this range of all members in the series. Apart from MSO₂Me-36, all the MOFs undergo pore filling above 0.4 P/P_0 . Changing the MC-MOF composition does not greatly affect the partial pressure at which the pore filling step occurs in these materials, as might be expected with having similar pore

sizes and functional groups. It is notable that the MOF with the highest humidity pore-filling step is MSO₂Pr-100. We ascribe this to the increased hydrophobicity of the slightly smaller pores lined with the longer propyl tails. Additionally, all the MC-MOFs showed similar maximum water uptake of approximately 11 water molecules per formula unit (Table 3). These results are understandable given the similar hydrophilic properties of the sulfoxide and sulfone functional groups and the similar sizes of the pores in the MOFs.

The water sorption isotherms show significant hysteresis and are not reversible. All the MOFs possess similar quantities of water remaining within their structures after desorption with a value of 2 molecules per formula unit (Table 3). These water molecules are likely to be binding to the metals in the structure and it is known that Zn₄O nodes are capable of binding additional ligands.^{30a, 32} The collapse of the MOFs to non-porous amorphous materials after the water vapor isotherms was confirmed by CO₂ adsorption (Figure S30) and PXRD measurements (Figure S31). Considering many IRMOFs suffer similar collapse in contact with moisture, this is unsurprising.^{13c, 17b, 24, 33}

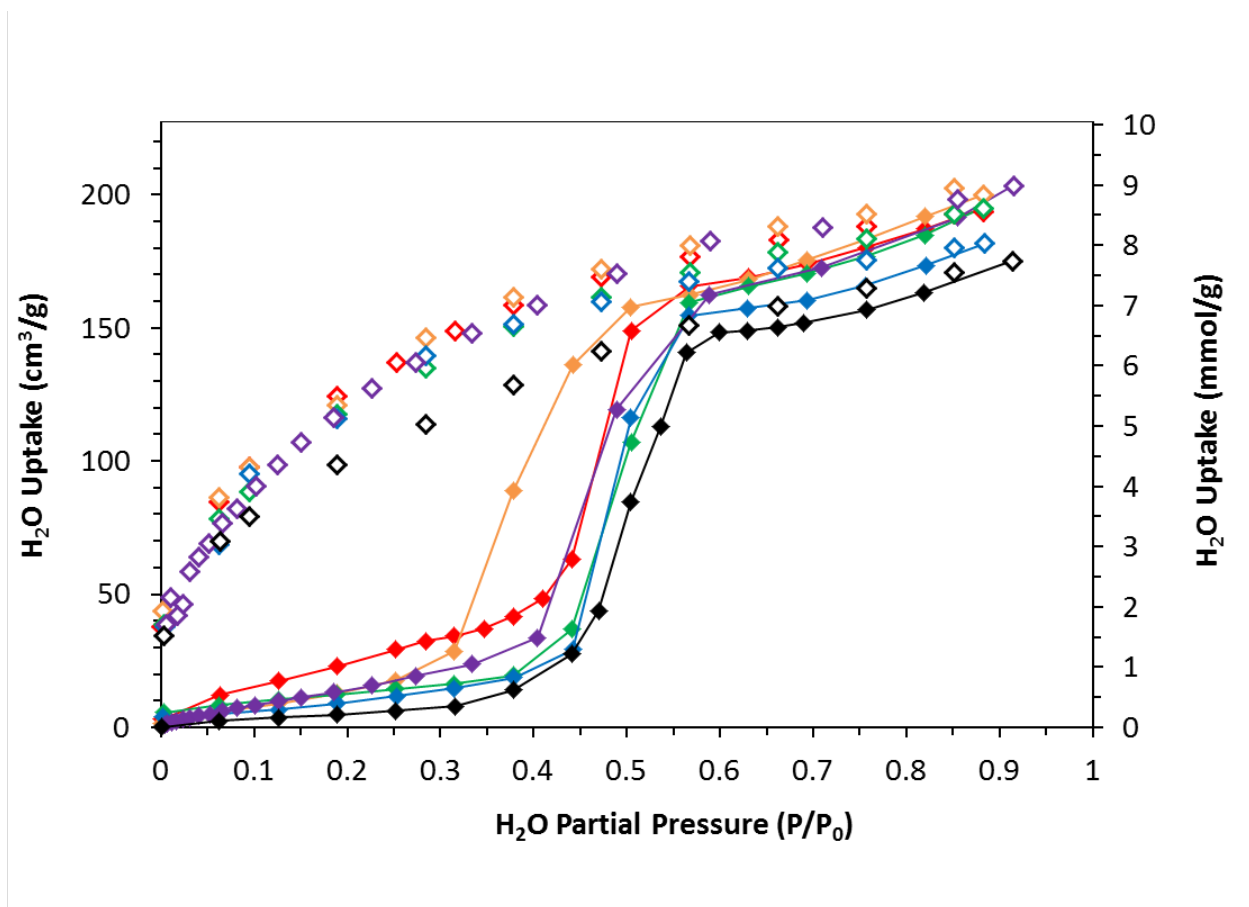


Figure 6. Water sorption isotherms for MSO₂Me-15 (red), MSO₂Me-36 (orange), MSO₂Me-64 (green), MSO₂Me-79 (blue), MSO₂Me-100 (purple) and MSO₂Pr-100 (black). Adsorption as closed symbols, with lines provided as guides for the eye, desorption as open symbols.

Table 3. Water uptake parameters of the MOFs at 298 K

<i>MOF</i>	<i>Total water uptake (mmol/g)</i>	<i>Water uptake in molecules per formula unit^a</i>	<i>Water remaining post-sorption (mmol/g)</i>	<i>Water remaining in molecules per formula unit</i>
MSO ₂ Me-15	8.6	10.6	1.7	2.1
MSO ₂ Me-36	8.8	11.0	1.9	2.4
MSO ₂ Me-64	8.6	10.8	1.7	2.1

MSO ₂ Me-79	8.0	10.1	1.7	2.1
MSO ₂ Me-100	9.0	11.4	1.7	2.2
MSO ₂ Pr-100	7.7	10.5	1.5	2.0

^a Formula unit based on framework formulations as in Table 1.

Conclusions

In summary, we have successfully synthesized a series of MC-IRMOF-9s with controlled ratios of sulfoxide and sulfone functionalities, in which the sulfoxide is obtained through *in situ* oxidation of a sulfide. This allowed us to systematically study the effects of ligand functionalization on gas and water sorption properties of this isostructural set of MOFs. The surface areas of the functionalized MC-IRMOF-9s are consistent and compare favorably to other IRMOF-9 type frameworks.^{30b, 34} Overall, the best properties for CO₂ adsorption came from MOFs carrying greater proportions of the sulfone functionality. MSO₂Me-100 gave the greatest CO₂ uptake at 1 bar and MSO₂Pr-100-Pr performed as well as MOFs with larger accessible surface areas and pore volumes. MSO₂Pr-100 gave the highest CO₂/N₂ selectivity which can be ascribed to a combination of pore constriction and increased hydrophobicity brought about by changing the sulfone alkyl chain from methyl to propyl. The enthalpies of CO₂ adsorption for the MC-MOF series range from 25-15 kJ mol⁻¹ with the highest enthalpy shown by MSO₂Me-79. These results all demonstrate the fine tuning possible through a ligand-directed MC approach.

The similar chemical functionality and pore diameters saw the water pore-filling step occur at roughly the same humidity for all the MC-MOFs, suggesting that the size of the pore is the primary parameter. However, changing the ligand tail from methyl to propyl pushed the pore filling step to higher humidity for MSO₂Pr-100.

In this series of functionalized IRMOF-9 compounds there are non-intuitive results. A complicating factor in the analysis is the subtleties of relative positioning and movements of the

interpenetrated frameworks and their associated functional groups upon activation and how this contributes to their performance. Despite these complexities the MC strategy is worth pursuing in order to discover advanced MOF materials.

ASSOCIATED CONTENT

Supporting Information. ^1H and ^{13}C NMR spectra for H_2L^4 and selected precursors, TG-DTA data, SCXRD data, PXRD patterns, gas sorption isotherms and information on surface area calculations. This material is available free of charge via the Internet at <http://pubs.acs.org>.”.

AUTHOR INFORMATION

Corresponding Author

* E-mail: chris_richardson@uow.edu.au

Author Contributions

The manuscript was written through contributions of all authors. All authors have given approval to the final version of the manuscript.

Funding Sources

Any funds used to support the research of the manuscript should be placed here (per journal style).

Notes

Any additional relevant notes should be placed here.

ACKNOWLEDGMENT

(Word Style “TD_Acknowledgments”). Generally the last paragraph of the paper is the place to acknowledge people, organizations, and financing (you may state grant numbers and sponsors here). Follow the journal’s guidelines on what to include in the Acknowledgments section.

ABBREVIATIONS

bdc, benzene dicarboxylate; bpdc, 4,4’ -biphenyl-dicarboxylate; bpy, 4,4’ -bipyridine; DMF, *N,N*’ -dimethylformamide; IRMOF, isorecticular metal-organic framework; MC, mixed-component; MOF, metal-organic framework; UiO, University of Oslo; MIL, Matériaux de l’Institut Lavoisier; NMR, nuclear magnetic resonance; PXRD, powder X-ray diffraction; SCXRD, single crystal X-ray diffraction; TG-DTA, thermogravimetric and differential thermal analysis; WUF, Wollongong University Framework;

REFERENCES

(Word Style “TF_References_Section”). References are placed at the end of the manuscript. Authors are responsible for the accuracy and completeness of all references. Examples of the recommended format for the various reference types can be found at <http://pubs.acs.org/page/4authors/index.html>. Detailed information on reference style can be found in *The ACS Style Guide*, available from Oxford Press.

1. (a) Yang, T.; Cui, H.; Zhang, C.; Zhang, L.; Su, C.-Y., *ChemCatChem*, 2013, 5, 3131-3138; (b) Leus, K.; Liu, Y.-Y.; Van Der Voort, P., *Cat. Rev.*, 2014, 56, 1-56.
2. Kreno, L. E.; Leong, K.; Farha, O. K.; Allendorf, M.; Van Duyne, R. P.; Hupp, J. T., *Chem. Rev.*, 2012, 112, 1105-1125.

3. (a) Couck, S.; Liu, Y.-Y.; Leus, K.; Baron, G. V.; Van der Voort, P.; Denayer, J. F. M., *Micropor. Mesopor. Mat.*, 2015, 206, 217-225; (b) Mondloch, J. E.; Katz, M. J.; Isley Iii, W. C.; Ghosh, P.; Liao, P.; Bury, W.; Wagner, G. W.; Hall, M. G.; DeCoste, J. B.; Peterson, G. W.; Snurr, R. Q.; Cramer, C. J.; Hupp, J. T.; Farha, O. K., *Nat Mater*, 2015, 14, 512-516; (c) Van de Voorde, B.; Bueken, B.; Denayer, J.; De Vos, D., *Chem. Soc. Rev.*, 2014, 43, 5766-5788.
4. (a) Zhang, M.; Bosch, M.; Gentle Iii, T.; Zhou, H.-C., *CrystEngComm*, 2014, 16, 4069-4083; (b) Farha, O. K.; Hupp, J. T., *Accounts Chem. Res.*, 2010, 43, 1166-1175.
5. (a) Wu, C.-D.; Hu, A.; Zhang, L.; Lin, W., *J. Am. Chem. Soc.*, 2005, 127, 8940-8941; (b) Gu, Z.-G.; Grosjean, S.; Brase, S.; Woll, C.; Heinke, L., *Chem. Commun.*, 2015; (c) Xamena, F. L. i.; Gascon, J., *Metal Organic Frameworks as Heterogeneous Catalysts*. The Royal Society of Chemistry: Cambridge, 2013.
6. (a) Meilikhov, M.; Yussenko, K.; Fischer, R. A., *J. Am. Chem. Soc.*, 2009, 131, 9644-9645; (b) Gui, B.; Yee, K.-K.; Wong, Y.-L.; Yiu, S.-M.; Zeller, M.; Wang, C.; Xu, Z., *Chem. Commun.*, 2015, 51, 6917-6920; (c) Lu, W.; Wei, Z.; Gu, Z.-Y.; Liu, T.-F.; Park, J.; Park, J.; Tian, J.; Zhang, M.; Zhang, Q.; Gentle Iii, T.; Bosch, M.; Zhou, H.-C., *Chem. Soc. Rev.*, 2014, 43, 5561-5593; (d) Wang, B.; Huang, H.; Lv, X.-L.; Xie, Y.; Li, M.; Li, J.-R., *Inorg. Chem.*, 2014, 53, 9254-9259; (e) Lammert, M.; Bernt, S.; Vermoortele, F.; De Vos, D. E.; Stock, N., *Inorg. Chem.*, 2013, 52, 8521-8528.
7. Cook, T. R.; Zheng, Y.-R.; Stang, P. J., *Chem. Rev.*, 2012, 113, 734-777.
8. (a) Sumida, K.; Rogow, D. L.; Mason, J. A.; McDonald, T. M.; Bloch, E. D.; Herm, Z. R.; Bae, T.-H.; Long, J. R., *Chem. Rev.*, 2011, 112, 724-781; (b) Li, J.-R.; Kuppler, R. J.; Zhou, H.-C., *Chem. Soc. Rev.*, 2009, 38, 1477-1504.

9. D'Alessandro, D. M.; Smit, B.; Long, J. R., *Angew. Chemie Int. Ed.*, 2010, 49, 6058-6082.
10. Das, A.; D'Alessandro, D. M., *CrystEngComm*, 2015, 17, 706-718.
11. (a) Yang, Q.; Wiersum, A. D.; Llewellyn, P. L.; Guillerm, V.; Serre, C.; Maurin, G., *Chem. Commun.*, 2011, 47, 9603-9605; (b) Meek, S. T.; Teich-McGoldrick, S. L.; Perry, J. J.; Greathouse, J. A.; Allendorf, M. D., *J. Phys. Chem. C*, 2012, 116, 19765-19772; (c) Biswas, S.; Zhang, J.; Li, Z.; Liu, Y.-Y.; Grzywa, M.; Sun, L.; Volkmer, D.; Van Der Voort, P., *Dalton Trans.*, 2013, 42, 4730-4737.
12. (a) Ko, N.; Hong, J.; Sung, S.; Cordova, K. E.; Park, H. J.; Yang, J. K.; Kim, J., *Dalton Trans.*, 2015, 44, 2047-2051; (b) De Lange, M. F.; Gutierrez-Sevillano, J.-J.; Hamad, S.; Vlugt, T. J. H.; Calero, S.; Gascon, J.; Kapteijn, F., *J. Phys. Chem. C*, 2013, 117, 7613-7622; (c) Han, S.; Huang, Y.; Watanabe, T.; Nair, S.; Walton, K. S.; Sholl, D. S.; Carson Meredith, J., *Micropor. Mesopor. Mat.*, 2013, 173, 86-91.
13. (a) Jasuja, H.; Burtch, N. C.; Huang, Y.-g.; Cai, Y.; Walton, K. S., *Langmuir*, 2012, 29, 633-642; (b) Yu, J.; Balbuena, P. B., *J. Phys. Chem. C*, 2013, 117, 3383-3388; (c) Kaye, S. S.; Dailly, A.; Yaghi, O. M.; Long, J. R., *J. Am. Chem. Soc.*, 2007, 129, 14176-14177.
14. (a) Burtch, N. C.; Jasuja, H.; Walton, K. S., *Chem. Rev.*, 2014, 114, 10575-10612; (b) Jasuja, H.; Jiao, Y.; Burtch, N. C.; Huang, Y.-g.; Walton, K. S., *Langmuir*, 2014, 30, 14300-14307; (c) Schoenecker, P. M.; Carson, C. G.; Jasuja, H.; Flemming, C. J. J.; Walton, K. S., *Ind. Eng. Chem. Res.*, 2012, 51, 6513-6519; (d) Liang, Z.; Marshall, M.; Chaffee, A. L., *Micropor. Mesopor. Mat.*, 2010, 132, 305-310.

15. Fracaroli, A. M.; Furukawa, H.; Suzuki, M.; Dodd, M.; Okajima, S.; Gándara, F.; Reimer, J. A.; Yaghi, O. M., *J. Am. Chem. Soc.*, 2014, 136, 8863-8866.
16. (a) Deria, P.; Mondloch, J. E.; Tylianakis, E.; Ghosh, P.; Bury, W.; Snurr, R. Q.; Hupp, J. T.; Farha, O. K., *J. Am. Chem. Soc.*, 2013, 135, 16801-16804; (b) Yu, C.; Bourrelly, S.; Martineau, C.; Saidi, F.; Bloch, E.; Lavrard, H.; Taulelle, F.; Horcajada, P.; Serre, C.; Llewellyn, P. L.; Magnier, E.; Devic, T., *Dalton Trans.*, 2015, 44, 19687-19692; (c) Noro, S.-i.; Matsuda, R.; Hijikata, Y.; Inubushi, Y.; Takeda, S.; Kitagawa, S.; Takahashi, Y.; Yoshitake, M.; Kubo, K.; Nakamura, T., *ChemPlusChem*, 2015, 80, 1517-1524.
17. (a) Cmarik, G. E.; Kim, M.; Cohen, S. M.; Walton, K. S., *Langmuir*, 2012, 28, 15606-15613; (b) Nguyen, J. G.; Cohen, S. M., 2010, 132, 4560-4561; (c) Liu, L.; Telfer, S. G., 2015, 137, 3901-3909.
18. (a) Burrows, A. D., 2011, 13, 3623-3642; (b) Zhang, Y.-B.; Furukawa, H.; Ko, N.; Nie, W.; Park, H. J.; Okajima, S.; Cordova, K. E.; Deng, H.; Kim, J.; Yaghi, O. M., *J. Am. Chem. Soc.*, 2015, 137, 2641-2650; (c) Burrows, A. D.; Fisher, L. C.; Richardson, C.; Rigby, S. P., *Chem. Commun.*, 2011, 47, 3380-3382; (d) Deng, H.; Doonan, C. J.; Furukawa, H.; Ferreira, R. B.; Towne, J.; Knobler, C. B.; Wang, B.; Yaghi, O. M., *Science*, 2010, 327, 846-850.
19. (a) Khutia, A.; Rammelberg, H. U.; Schmidt, T.; Henninger, S.; Janiak, C., *Chem. Mater.*, 2013; (b) Reinsch, H.; Waitschat, S.; Stock, N., *Dalton Trans.*, 2013, 42, 4840-4847.
20. Horike, S.; Inubushi, Y.; Hori, T.; Fukushima, T.; Kitagawa, S., *Chem. Sci.*, 2012, 3, 116-120.

21. Yang, J.; Grzech, A.; Mulder, F. M.; Dingemans, T. J., *Eur. J. Inorg. Chem.*, 2013, 2013, 2336-2341.
22. Park, T.-H.; Koh, K.; Wong-Foy, A. G.; Matzger, A. J., *Cryst. Growth Des.*, 2011, 11, 2059-2063.
23. Burrows, A. D.; Frost, C. G.; Mahon, M. F.; Richardson, C., *Chem. Commun.*, 2009, 4218-4220.
24. Bryant, M. R.; Richardson, C., *CrystEngComm*, 2015.
25. Wade, C. R.; Corrales-Sanchez, T.; Narayan, T. C.; Dinca, M., 2013, 6, 2172-2177.
26. (a) Halis, S.; Reimer, N.; Klinkebiel, A.; Lüning, U.; Stock, N., *Micropor. Mesopor. Mat.*, 2015; (b) Neofotistou, E.; Malliakas, C. D.; Trikalitis, P. N., *Chem. Eur. J.*, 2009, 15, 4523-4527.
27. (a) Julian, H.; Wenten, I. G., *IOSR JE*, 2012, 2, 484-495; (b) Weigang Lu; Daqiang Yuan; Julian Sculley; Dan Zhao; Rajamani Krishna; Zhou, H.-C., *J. Am. Chem. Soc.*, 2011, 133, 18126-18129.
28. FSProcess, Rigaku Corporation: Tokyo, Japan, 1996.
29. Sheldrick, G., 2008, 64, 112-122.
30. (a) Burrows, A. D.; Frost, C. G.; Mahon, M. F.; Richardson, C., *Angew. Chem., Int. Ed.*, 2008, 47, 8482-8486; (b) Burrows, A. D.; Hunter, S. O.; Mahon, M. F.; Richardson, C., *Chem. Commun.*, 2013, 49, 990-992; (c) Roberts, J. M.; Farha, O. K.; Sarjeant, A. A.; Hupp, J. T.;

Scheidt, K. A., 2011, 11, 4747-4750; (d) Burrows, A. D.; Frost, C. G.; Mahon, M. F.; Richardson, C., 2009, 0, 4218-4220.

31. Tshering, L.; Hunter, S. O.; Nikolich, A.; Minato, E.; Fitchett, C. M.; D'Alessandro, D. M.; Richardson, C., CrystEngComm, 2014, 16, 9158-9162.

32. (a) Hausdorf, S.; Wagler, J. r.; Moßig, R.; Mertens, F. O. R. L., J. Phys. Chem. A, 2008, 112, 7567-7576; (b) Schrock, K.; Schroder, F.; Heyden, M.; Fischer, R. A.; Havenith, M., 2008, 10, 4732-4739; (c) Akimbekov, Z.; Wu, D.; Brozek, C. K.; Dinca, M.; Navrotsky, A., 2016, 18, 1158-1162; (d) Bellarosa, L.; Brozek, C. K.; García-Melchor, M.; Dincă, M.; López, N., 2015, 27, 3422-3429; (e) Greathouse, J. A.; Allendorf, M. D., 2006, 128, 10678-10679.

33. Bury, W.; Justyniak, I.; Prochowicz, D.; Wrobel, Z.; Lewinski, J., Chem. Commun., 2012, 48, 7362-7364.

34. Babarao, R.; Coghlan, C. J.; Rankine, D.; Bloch, W. M.; Gransbury, G. K.; Sato, H.; Kitagawa, S.; Sumby, C. J.; Hill, M. R.; Doonan, C. J., Chem. Commun., 2014, 50, 3238-3241.